Research Article

For reprint orders, please contact reprints@futuremedicine.com

Nanomedicine

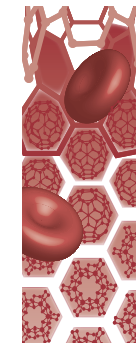

Enhanced selective sonosensitizing efficacy of ultrasound-based anticancer treatment by targeted gold nanoparticles

Aim: This study investigates cancer targeted gold nanoparticles as ultrasound sensitizers for the treatment of cancer. Methods: The ultrasound sensitizer activity of folate-PEG decorated gold nanoparticles (FA-PEG-GNP) has been studied on human cancer cell lines that overexpress folate receptors (KB and HCT-116) and another that does not (MCF7), at two ultrasound energy densities (8×10^{-6} J cm^{-2} and 8×10^{-5} J cm^{-2}, for 5 min at 1.866 MHz). Results: FA-PEG-GNP selectively targeted KB and HCT-116 cells and a remarkable reduction in cancer cell growth was observed upon ultrasound exposure, along with significant reactive oxygen species generation and increase in necrotic cells. Conclusion: The combined use of targeting capacity and the ultrasound sensitizing effect, make FA-PEG-GNP promising candidates for the site-specific cancer treatment.

First draft submitted: 3 August 2016; Accepted for publication: 30 August 2016; Published online: 15 September 2016

Keywords: cancer • cancer targeting • gold nanoparticles • nanosonosensitizer • sonodynamic treatment • sonosensitizer • therapeutic ultrasound

Chiara Brazzale[1], Roberto Canaparo*[,2], Luisa Racca[2], Federica Foglietta[2], Gianni Durando[3], Roberto Fantozzi[2], Paolo Caliceti[1], Stefano Salmaso**[,1] & Loredana Serpe[2]

[1]Department of Pharmaceutical & Pharmacological Sciences, University of Padova, Via F. Marzolo 5, 35131 Padova, Italy

[2]Department of Drug Science & Technology, University of Torino, Via P. Giuria 13, 10125 Torino, Italy

[3]National Institute of Metrological Research (INRIM), Strada delle Cacce 91, 10135 Torino, Italy

*Author for correspondence:
Tel.: +39 0116706235
Fax: +39 0116706230
roberto.canaparo@unito.it

**Author for correspondence:
Tel.: +39 0498271602
Fax: +39 0498275366
stefano.salmaso@unipd.it

Ultrasound (US) can affect the functional and structural properties of biological tissues via a number of mechanisms, generally classified as thermal or nonthermal, which are dependent on factors such as frequency, pressure, power and exposure time [1,2]. The effects of US can be exploited for therapeutic purposes. The thermal anticancer applications of US, such as high intensity focused ultrasound which induces coagulative necrosis at a precise focal point [3], have been more extensively studied than the therapeutic uses of the nonthermal US effects. The effects of US on tissue include, other than the direct thermal effect: alteration of biobarrier permeability, drug delivery and sonodynamic activity [1]. The last effect has recently been the driving force behind a great deal of interest, as the peculiar phenomenon of cavitation is opening new perspectives for cancer treatment [4]. US-induced inertial cavitation generates gas bubbles that grow to near resonance size and expand to a maximum before collapsing violently with the conversion of the diffused energy into highly localized heat and pressure. Bulk temperature and pressure within the imploding cavities can reach values of up to 10,000°K and 800 atm, respectively. These extreme conditions can induce a variety of physical events both within and around the bubble, including an increase in energy density that can generate light: a phenomenon known as sonoluminescence [5,6]. Furthermore, US-induced inertial cavitation can transfer energy to surrounding molecules and alter their chemical properties, yielding sonosensitizers and finally cancer cell death. Therefore, the combination of US-induced inertial cavitation and sonosensitizing agent has been defined sonodynamic therapy (SDT) [7,8].

Although the SDT mechanism is still a matter of much debate, it is generally accepted that the main effectors of sonosensitised cell damage are short-lived chemical

Future Medicine part of fsg

species, namely reactive oxygen species (ROS) and free radicals, generated as a consequence of the selective accumulation of the sonosensitizing agent in tumors and triggered by US-induced acoustic cavitation [9]. Therefore, SDT can be exploited as a 'remotely controlled' bimodal therapeutic treatment, in which, a nontoxic molecule or system (chemical actuator), in other words, the sonosensitizer, is activated by US (physical activator) yielding oxidative damage and consequent cancer cell death.

SDT is thus achieved by an external physical stimulus that activate molecules or colloidal systems yielding, in turn, a biological effect only when the former and the latters are combined together. Accordingly, SDT has similar potential to photodynamic therapy (PDT), a clinically approved bimodal anticancer approach, where light is used to activate particular chemical compounds, in other words, photosensitizers, to kill cancer cells. Nevertheless, PDT has some drawbacks, the most important of which being the poor diffusion of light through human tissues, even at long wavelengths in the near-infrared (NIR). This limits PDT's application to superficial tumor treatment [10,11]. As US easily propagates through the body, allowing the targeting of more deeply-seated cancer lesions without the need for invasive devices, STD can be a promising approach to overcome this drawback [4].

Although SDT appears to be an encouraging new approach for cancer therapy, significant progresses in the field will depend on the development of US specific sonosensitizers that can efficiently convert US-induced cavitation into ROS production within the tumor tissue in a US-dose dependent manner. In this regard, nanoparticle-based sonosensiter delivery system can assure the safe delivery and selective action of well-known sonosensitizers to the target site [12–14]. However, inorganic-based nanoparticles might also be able to play themselves as sonosensitizer role, taking advantage of their unique features. This has triggered an increased interest in the development of innovative nanosonosensitizers such as carbon nanoparticles [15,16], silicon nanoparticles [17–19] and titanium dioxide nanoparticles [20–22].

Gold nanoparticles (GNPs) have been brought to the forefront of cancer research in recent years because they are easily produced and can support great versatility in their surface coatings. Furthermore, GNP posses tunable optical and thermal properties as well as high biocompatibility that make them suitable systems for clinical application [23–25]. Moreover, the GNP plasmonic effect that derives from surface plasmon resonance (SPR), a unique photophysical response to light in which the oscillating electromagnetic field of light induces a collective coherent oscillation of free electrons (conduction band electrons) in a metal, distinguishes them from other nanosystems [26]. This SPR effect, which results from photon confinement to a small particle size, is also correlated to some nanoparticle properties including their radiative, absorption and scattering, and nonradiative, the quick conversion of strongly absorbed light to heat, properties [27]. Since GNP absorb light millions of times more intensely than organic dyes [26], they have already been proposed for photothermal therapy, a treatment for shallow cancer (e.g., skin cancer) in which photon energy is converted to heat in order to induce cellular damage via hyperthermic effects [28].

Their good uptake by mammalian cells, their low toxicity, their peculiar interaction with light (i.e., SPR) and the sonoluminescence hypothesis underlining STD, all make GNP ideal candidates for use as sonosensitizing agents in SDT and also provide the drive for a step forward for clinical applications in this field.

We have developed folic acid conjugated gold nanoparticles (FA-PEG-GNP) in order to further improve the site-specificity of the sonodynamic treatment of cancer. The enhanced specificity and intracellular access of these systems has led to the active targeting of colloidal therapeutic systems attracting considerable interest [24,29–31]. Folic acid (FA), a low molecular weight vitamin, is a typical cell-targeting agent in virtue of its binding affinity toward the folate receptor (FR) that is known to be over-expressed by a variety of human cancer cells. Moreover, the FR distribution appears to rise as cancer progress, whereas FR is only minimally distributed in normal cells [32,33].

Notably, particles were surface coated with PEG, which can provide for colloidal stability and prevent the opsonization process in vivo. Accordingly, PEGylated nanoparticles long circulate in the bloodstream thus favoring their biodistribution to the tumor tissue while reducing off-target accumulation [34]. However, a few studies have shown that GNP can be cleared from the body thus preventing accumulation-associated toxicity. GNP with size of 10–250 nm are cleared through the hepatobiliary system [35,36] by a complex combination of processes, which include the cellular exocytosis of the nanoparticles internalized in healthy tissue cells and mononuclear phagocytic system of the liver [37]. The exocytosis mechanisms and rates of GNP have been found to depend on their surface properties, size and shape as well as on the cell type [38,39]. Therefore, even though more investigations are required to extensively elucidate the in vivo fate of gold particles, the fine design of their features, namely size and surface decoration, is paramount to produce systems with required in vivo behavior.

This work aims to provide a proof-of-concept study for the use of targeted GNP as site-selective nanosono-

sensitizers for ultrasound triggered cancer cell death since, to the best of our knowledge, such an attempt has not yet been reported.

Materials & methods

Materials

Dicyclohexylcarbodiimide, N-hydroxysuccinimide (NHS), triethylamine, folic acid, 5,50-dithio-bis(2-nitrobenzoic acid) (DTNB), Tris(2-carboxyethyl) phosphinehydrochloride,sodiumcitratedihydrateand tetrachloroauric(III) acid, fetal bovine serum, RPMI 1640, McCoy's 5A, FFDMEM, glutamine solution, penicillin-streptomycinsolution,glucosesolutionandtrypsin-EDTA solution were all purchased from Sigma (MO, USA). The sephadex G25 superfine resin was obtained from Pharmacia Biotech AB (Uppsala, Sweden). mPEG-$_{2kDa}$-SH and NH_2-$PEG_{3.5kDa}$-SH were purchased from Iris Biotech GmbH (Marktredwitz, Germany). Spectra/Por Float-a-lyzer G2 (MW cutoff = 0.5–1 kDa) was obtained from Spectrumlabs (CA, USA).

Synthesis of folate-$PEG_{3.5\ kDa}$-SH

Folic acid (50.0 mg, 0.113 mmol) was dissolved in 1 ml of anhydrous DMSO. NHS (15.6 mg, 0.136 mmol) followed by dicyclohexylcarbodiimide (28.1 mg, 0.136 mmol) were added to the solution. The mixture was stirred overnight in the dark and then filtered to remove the insoluble dicyclohexylurea. N-hydroxysuccinimidyl-ester-activatedfolicacidwasisolatedby precipitation in cold diethyl ether. The precipitate was washed several times with cold diethyl ether. The NHS ester activated folic acid was then dried under reduced pressure. NHS-folic acid (25 mg, 0.046 mmol) and NH_2-$PEG_{3.5kDa}$-SH (54.1 mg, 0.015 mmol) were dissolved in 1 ml of anhydrous DMSO, with the addition of triethylamine (2.1 µl, 0.015 mmol). The reaction mixture was stirred for 12 h at room temperature in the dark and then added dropwise to diethyl ether (40 ml). The precipitate was recovered by centrifugation and dried under vacuo. The crude product was purified from the unreacted folic acid using size exclusion chromatography and a Sephadex G-25 resin eluted with an aqueous ammonia solution (pH 9). The column fractions were tested using UV-Vis spectroscopy at 363 nm and the iodine test [40] to assess folate and PEG, respectively. The fractions that were positive in both assays were collected and freeze-dried. The yellow powder was treated by reduction in order to regenerate free thiol groups. The material (20 mg, corresponding to 8.2 µmoles of FA-$PEG_{3.5kDa}$-SH) and TCEP (20.5 mg, 82 µmoles) were dissolved in 50 mM acetate buffer at pH 5 and left under stirring for 3 h. The mixture was then dialyzed using a Spectra/Por Float-a-lyzer G2 (MW cutoff = 0.5–1 kDa) with a 1 mM HCl, 1 mM EDTA solution as the releasing medium. The dialysis was performed for 2 days and then the FA-$PEG_{3.5kDa}$-SH solution was then freeze-dried.

The lyophilized FA-$PEG_{3.5kDa}$-SH was dissolved in phosphate-buffered saline (PBS) pH 7.4 and analyzed using UV-Vis spectroscopy at 363 nm (molar extinction coefficient of folate at 363 nm in PBS, pH 7.4 is 6.197 $M^{-1}\ cm^{-1}$ [41]) and iodine test to assess the conjugation efficiency, and using the Ellman's assay [42] to determine the percentage of free thiol groups. FA-$PEG_{3.5kDa}$-SH was characterized using MALDI mass spectroscopy on a 400 Plus MALDI TOF/TOF Analyzer (AB Sciex, MA, USA).

Product purity was evaluated using reverse phase chromatographic analysis on a Jasco HPLC system (Tokyo, Japan), equipped with two PU-2080 Plus pumps, a UV-2075 Plus detector (set at 363 nm), an analytic column Luna (C18, 5 µ, 300 Å, 250 × 4.6 mm) from Phenomenex (CA, USA) and eluted in gradient mode with 10 mM Mammonium acetate buffer, pH 6.5 (eluent A) and acetonitrile (eluent B). Eluent B was increased linearly from 10 to 40% over 40 min.

^{1}H NMR (300 MHz, DMSO-d_6): δ 8.64 (s, C7-H of FA, 1H), 7.64 (d, 2′,6′-H of FA, 2H), 6.65 (d, 3′,5′-H of FA, 2H), 4.35–4.26 (m, α-CH of Glu of FA, 1H), 3.50 (s, PEG, ~316H), 2.89 (t, CH_2-S, 2H).

GNP preparation

The preparation of GNP was performed according to the Turkevich method [43] using sodium citrate as the reducing and capping agent. Glassware was extensively washed with aqua regia (3:1 v/v of 12.2 M hydrochloric acid/14.6 M nitric acid) and then rinsed with deionized water. A 0.25 mM tetrachloroauric solution was prepared in Milli-Q water (100 ml) and heated up to 75°C under stirring. Trisodium citrate dihydrate (100 mg) was dissolved in Milli-Q water and 3 ml of the solution (0.34 M) was added dropwise to the $HAuCl_4$ solution. The mixture was left under stirring for 1 h. Then, the gold colloidal suspension was cooled to room temperature and extensively characterized.

A 18 µl volume of a 0.5 mg/ml FA-$PEG_{3.5kDa}$-SH aqueous solution was mixed with 9 µl of a 50 µg/ml mPEG$_{2kDa}$-SH aqueous solution. The polymer mixture was immediately added to 15 ml of a 3 nM GNP suspension to a final 50:5:1 FA-$PEG_{3.5kDa}$-SH/mPEG$_{2kDa}$-SH/GNP molar ratio. The suspension was left under rotational stirring overnight at room temperature. Then the mixture was centrifuged at 14,000 r.p.m. for 30 min at 4°C to isolate the particles and the supernatant was lyophilized and redissolved in 150 µl of Milli-Q water and analysed by UV-Vis spectroscopy at 363 and 535 nm (iodine test) to assess the quantity of unbound FA-$PEG_{3.5kDa}$-SH and mPEG$_{2kDa}$-SH.

The particle pellet was washed three times with Milli-Q water and resuspended in 15 ml of Milli-Q water. The particle suspension was then added of 72 µl of 5 mg/ml $mPEG_{2kDa}$-SH aqueous solution in order to extensively decorate the particle surface with the thiolated methoxy-PEG-SH ($mPEG_{2kDa}$-SH/GNP molar ratio = 4000:1). The mixture was left overnight under rotational stirring. The resulting suspension of folate coated PEGylated GNPs (FA-PEG-GNP) was centrifuged at 14,000 r.p.m. for 30 min at 4°C. The FA-PEG-GNP pellet was isolated from the supernatant, which was subsequently analyzed using the iodine test to assess the quantity of unbound PEG.

Control nontargeted particles (mPEG-GNP) were produced using $mPEG_{3.5kDa}$-SH instead of FA-$PEG_{3.5kDa}$-SH and surface was saturated with $mPEG_{2kDa}$-SH using the same $mPEG_{3.5kDa}$-SH/$mPEG_{2kDa}$-SH/GNP molar ratio (50:650:1) and procedure reported above.

GNP characterization

DLS analysis

The size of naked and functionalized GNP was measured at 25°C using dynamic light scattering (DLS) on a Zetasizer NanoZS (Malvern Instruments Ltd, UK) equipped with a red laser (633 nm) at a fixed angle of 173°. 'DTS applications 6.12' software was used to analyze the data. All sizes reported were based on number average.

TEM analysis

Transmission electron microscopic (TEM) imaging was performed on a Tecnai G2 microscope (FEI Tecnai, OR, USA). Ten microliters of naked particle suspension (1 nM) in milli-Q water were placed on a carbon-coated copper grid and the water was allowed to dry at room temperature. The average particle size was calculated from the average of 100–300 individual particle diameters using 'SIS Soft Imaging GmbH' image analysis software. The targeted particles (FA-PEG-GNP) and control PEGylated particles (mPEG-GNP) were negatively stained with 1% uranyl acetate dissolved in distilled water and analyzed according to the same protocol.

Concentration assessment

The concentrations of GNP suspensions were assessed according to the method reported by Liu et al. [44]. Equation (1) was applied to derive the particle molar extinction coefficient, which referred to absorbance at 506 nm (ε_{506}):

$$\ln \varepsilon = k \ln D + a$$

where D is the diameter of the nanoparticles (obtained from DLS analysis), k and a are two constants whose values are 3.32111 and 10.80505, respectively [45,46]. ε_{506} was then used to calculate the particle concentration according to the Lambert–Beer law.

Cell culture

Human MCF7 breast adenocarcinoma (ICLC, Interlab Cell Line Collection, Genova, Italy), HCT-116 colon carcinoma (ICLC) and KB epidermoid carcinoma (ECACC, European Collection of Cell Culture, Salisbury, UK) cell lines were cultured as monolayer in RPMI 1640, McCoy's 5A and folate-free DMEM (FFDMEM) growth medium, respectively, supplemented with 10% fetal bovine serum (v/v), 2.0 mM L-glutamine, 100.0 UI/ml penicillin and 100.0 µg/ml streptomycin in a humidified atmosphere containing 5% CO_2 at 37°C. Cells were detached using 0.05% trypsin-0.02% EDTA solution (Sigma), suspended in culture medium and seeded at the appropriate cell concentrations for cell culture experiments.

Cell folate receptor expression

In order to assess folate receptor expression on cell lines, 1.0×10^3 MCF7, 0.4×10^3 HCT-116, 0.7×10^3 KB cells were cultured in 6-well culture plates (Techno Plastic Products, Trasadingen, Switzerland) in 2 ml of respective culture medium. After 72 h, cells were incubated with 10 µg/ml folate receptor α monoclonal antibody (Enzo Life Science, NY, USA) for 2 h at 37°C. Cells were then washed with PBS (PBS, pH 7.4, 150 mM) and incubated with 0.5 µl/ml rabbit F(ab')2 polyclonal secondary antibody-Alexa Fluor® 488 (Abcam, Cambridge, UK) for 1 h at 37°C [47]. Finally, cells were trypsinized, normalized to 5.0×10^5 cells in 0.3 ml of PBS and analyzed on a C6 flow cytometer (Accuri Cytometers, Inc., MI, USA) and a total of 10,000 events were recorded. Results were expressed as integrated mean fluorescence intensity (iMFI), defined as the percentage of FR-positive cells multiplied by the mean fluorescence intensity of FR-positive cells.

Cell uptake studies

MCF7, HCT-116 and KB cells were seeded in 12-well plates (500 µl per well, 1×10^6 cells/ml) and grown for 24 h. The medium was removed, cells washed twice with PBS and either 1 nM FA-PEG-GNP or control nontargeted mPEG-GNP suspensions in FFDMEM were added (1 ml/well). After 2 h of incubation at 37°C, the particle containing media were removed and the cells were washed three-times with PBS without $MgCl_2$ and $CaCl_2$. The cells were then detached using 1% w/v trypsin treatment (150 µl/well). Trypsin was quenched by adding 500 µl of PBS containing $MgCl_2$ and $CaCl_2$ to each well and cells were recovered by centrifugation at 1000 r.p.m. for 5 min. The cell pellets were washed twice with PBS and then a 0.1 w/v% Triton® X-100

solution in water (600 µl) was added and exposed to sonication for 1 h. The samples were then centrifuged at 1000 r.p.m. for 5 min and number of cells per sample was assessed on 100 µl of the cell lysate using the BCA Protein Assay Kit (Thermo Fisher Scientific Inc., MA, USA). Five hundred microliters of cell lysate were digested by aqua regia treatment (5 ml) at 80°C for 1 h to dissolve gold. The mineralized lysates were suitably diluted with 0.32 M HCl and analyzed by Atomic Absorption Spectroscopy to assess gold concentration on a Varian AA240 Zeeman instrument equipped with a GTA120 graphite furnace, a Zeeman background corrector and an autosampler (Varian, Inc., CA, USA). Nanoparticles number per cell were derived from gold concentration and the number of cells in the samples.

Cell uptake inhibition assay

MCF7, HCT-116 and KB cells seeded in 12-well plates were washed twice with PBS and incubated with 1 nM FA-PEG-GNP or 1 nM mPEG-GNP suspensions in FFDMEM medium supplemented with free folic acid (200 µM). After an incubation time of 2 h at 37°C, the cell samples were processed as mentioned above for gold quantification by atomic absorption analysis.

TEM

The intracellular disposition of GNP was imaged using TEM analysis. KB cells were seeded at a density of 3×10^5 in 12-well plates in FFDMEM as reported above. After 24 h, the cells were washed twice with PBS and incubated for 2 h with either a 1 nM FA-PEG-GNP or a mPEG-GNP suspension in FFDMEM medium. The medium was then removed from the wells and the cells were washed three-times with PBS and fixed by treatment with 2.5 w/v% glutaraldehyde in 0.1 M sodium cacodylate buffer at 4°C for 1 h. The cells were washed twice with sodium cacodylate buffer and post fixed in 0.1 M sodium cacodylate buffer containing 1 w/v% osmium tetroxide for 1 h. Each sample underwent a dehydration treatment with ethanol and samples were embedded in fresh EPON resin. Ultrathin sections of the resin embedded samples were cut and imaged on a Tecnai G2 Transmission Electron Microscope (FEI Tecnai).

Ultrasound treatment

Cells in the exponential growth phase were incubated for 2 h in FFDMEM medium containing either 1 nM of FA-PEG-GNP or the control, nontargeted mPEG-GNP suspension. Cells were then washed with PBS, trypsinized and normalized to 5.0×10^5 cells in 2.5 ml of PBS in polystyrene tubes for US exposure.

The US field was generated by a plane wave transducer (2.54 cm diameter) in continuous wave, in other words, CW mode, at f_0 = 1.866 MHz connected to a power amplifier (Type AR 100A250A; Amplifier Research, PA, USA) and a function generator (Type 33250; Agilent, CA, USA). A mechanical adaptor was built to connect the 1 cm diameter polystyrene tube containing the cells suspended in PBS. When filled with ultrapure water, the adaptor creates highly reproducible measurement conditions at a fixed cell tube distance from the transducer (17 mm) [48].

US exposure was performed for 5 min, under a dim light, at two different energy densities: US_n, corresponding to 0.008 mJ/cm^2 energy supplied to the cells which did not cause the temperature of the medium to increase (maximum temperature recorded was 33°C) and US_t, corresponding to 0.080 mJ/cm^2 energy supplied to the cells which increased the temperature of the medium (maximum temperature recorded was 43°C).

Cell proliferation assay

The WST-1 cell proliferation assay (Roche Applied Science, Penzberg, Germany) was used to evaluate the effects of treatment on cell growth. After the various treatments, 2.5×10^3 MCF7, 1.5×10^3 HCT-116 and 2.0×10^3 KB cells were seeded in 100 µl of culture medium in replicates (n = 8) for each condition in 96-well culture plates (TPP, Trasadingen, Switzerland). MCF7 and HCT-116 cells were incubated for 1.5 h and KB cells for 2 h with WST-1 reagent (10 µl) at 37°C, 24, 48 and 72 h after the US treatment. Well absorbance was measured at 450 and 620 nm (reference wavelength) on a microplate reader (Asys UV340; Biochrom, Cambridge, UK). Cell proliferation data were expressed as a percentage of untreated cells.

Folic acid uptake competition assay

HCT-116 and KB cells were also incubated with FFDMEM medium containing 1.0 nM FA-PEG-GNP suspension and 200 µM folic acid (Sigma) for 2 h to evaluate the uptake selectivity of FA-PEG-GNP by cell folate receptor under competition conditions with folic acid. Cells were then detached and subjected to US treatment as previously described; cell growth was evaluated using a WST-1 assay after 24, 48 and 72 h.

ROS scavenging assay

HCT-116 and KB cells were incubated with the ROS scavenger N-acetyl-cysteine (NAC; Sigma) in order to evaluate ROS involvement in cell proliferation upon targeted GNP incubation and US treatment. Briefly, cells were incubated with 1.0 nM FA-PEG-GNP suspension in FFDMEM medium for 2 h and 5.0 mM NAC was added after 1 h of incubation. Cells were then trypsinized, washed with PBS and exposed to US. Cell growth was assessed using a WST-1 assay after 24, 48 and 72 h.

Cell death analysis

HCT-116 and KB cell death was investigated using the Dead Cell Apoptosis Kit with allophycocyanin (APC)-Annexin V and Sytox® Green (Life Technologies, Milan, Italy) with an Accuri C6 flow cytometer. Cells were incubated for 2 h in FFDMEM medium containing 1.0 nM FA-PEG-GNP suspension, cells were then trypsinized, washed with PBS and normalized to 5.0×10^5 cells in 2.5 ml of PBS for US treatment. After US exposure, cells were collected into 3 ml sterile centrifuge tubes for 2 h, washed twice with 1 × Annexin-binding buffer at 1500 r.p.m. for 5 min and stained with APC-Annexin V and Sytox Green for 15 min at 37°C and samples underwent flow cytometric analyses. Cell debris with low forward light scatter and side light scatter were excluded from the analyses and a total of 10,000 events were analyzed. Fluorescence was collected at 660 and 530 nm to discriminate APC-Annexin V and Sytox Green signals, respectively. Apoptotic and late apoptotic/necrotic cells were discriminated from viable cells using the FCS Express software, version 4 (BD, Bioscience, Milano, Italy).

Intracellular ROS production analyses

Intracellular ROS generation was measured using the 2,7-dichlorodihydrofluorescein diacetate (DCFH-DA; Sigma) probe with a C6 flow cytometer. Briefly, HCT-116 and KB cells were incubated with a 1.0 nM FA-PEG-GNP suspension in FFDMEM medium for 2 h and 10 μM DCFH-DA for the last 30 min at 37°C. Cells were then PBS washed, trypsinized and exposed to US as previously described. ROS production was measured at 1, 5, 15, 30 and 60 min after each treatment and a total of 10,000 events were recorded in the flow cytometric analysis. ROS production was expressed as iMFI, which was calculated as the product of the frequency of ROS-producing cells and the median fluorescence intensity of the cells. The iMFI ratio was calculated in order to yield the ratiometric increase in fluorescence per time point.

The ROS generation in HCT-116 and KB cells treated with FA-PEG-GNP and US was also assessed in the presence of the ROS scavenger, NAC. Briefly, cells were incubated at 37°C with a 1 nM FA-PEG-GNP suspension in FFDMEM medium for 2 h, then 5.0 μM NAC was added after 1 h of incubation and 10 μM DCFH-DA after 1.5 h of incubation. Cells were then PBS washed, trypsinated, treated with US and ROS production was assessed using flow cytometric analysis, as previously described.

Statistical analysis

Data are shown as the average values ± standard deviation of three independent experiments. Statistical analyses were performed using Graph-Pad Prism 6.0 software (CA, USA); two-way analysis of variance and Bonferroni's test were used to calculate the threshold of significance. Statistical significance was set at $p < 0.05$.

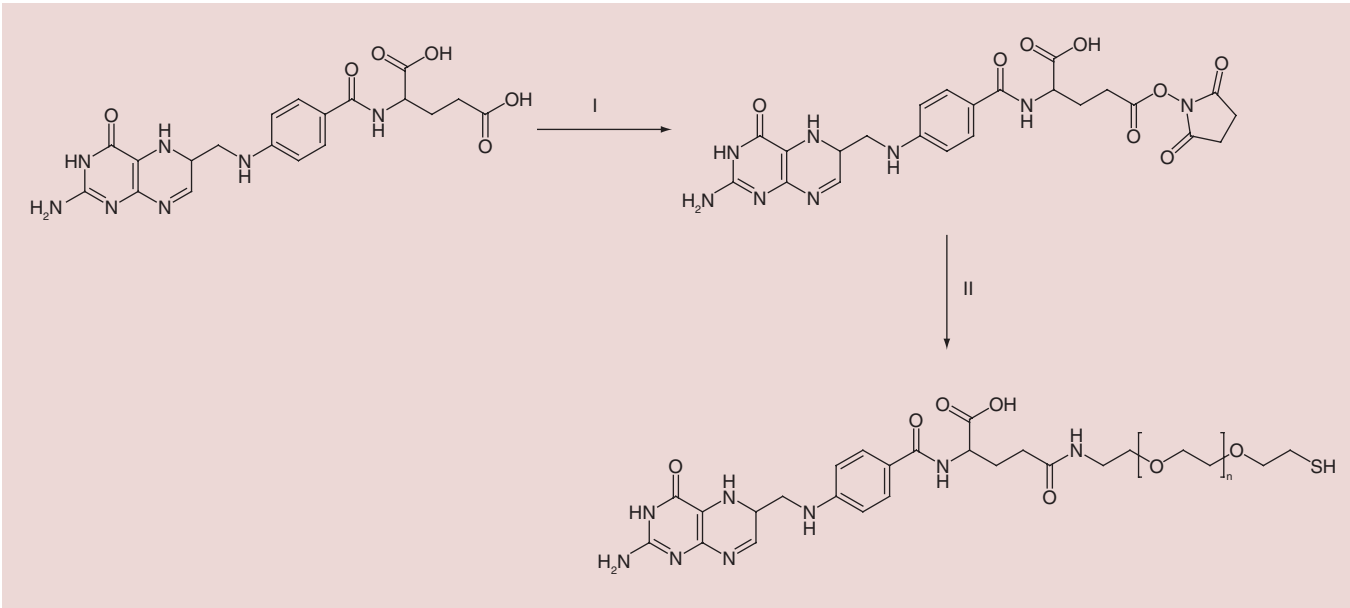

Figure 1. Synthesis of folate-$PEG_{3.5kDa}$-SH. Activation of folic acid carboxyl group by NHS and dicyclohexylcarbodiimide in anhydrous DMSO and conjugation of NHS-ester activated folate to NH_2-$PEG_{3.5kDa}$-SH in anhydrous DMSO in presence of TEA. NHS: N-hydroxysuccinimide.

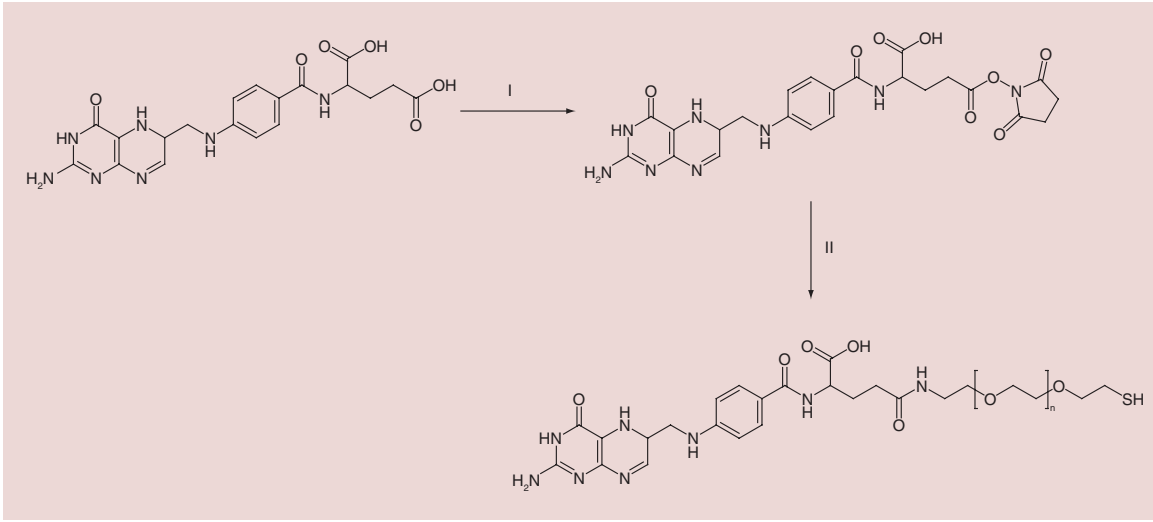

Figure 2. MALDI-TOF spectrum of (A) NH_2-PEG-SH and (B) FA-PEG-SH conjugate.
FA-PEG-SH: Folate-$PEG_{3.5kDa}$-SH.

Results

Synthesis & characterization of folate-$PEG_{3.5kDa}$-SH

Folate-$PEG_{3.5kDa}$-SH (FA-PEG-SH) conjugate was synthesised according to the method reported in the literature [49] (Figure 1).

Conjugate was purified from unreacted NHS-folate by gel filtration and then treated with TCEP to reduce the oxidized diemeric species (FA-PEG-S-S-PEG-FA). The TCEP treatment yielded 96% of -SH groups that were available for the conjugation to the GNP surface. Spectrophotometric analyses gave an NH_2-PEG-SH to folic acid coniugation efficiency of 98%. FA-PEG-SH showed MALDI-TOF mass spectrum (Figure 2B) with the typical bell shaped profile for PEG, which was centerd at 4000 m/z and was in agreement with the expected molecular weight of the conjugate (Figure 2). This result confirmed that the product contained only the FA-PEG-SH monomer. In fact, no traces of either NH_2-PEG-SH or the dimer (FA-PEG-S-S-PEG-FA) were detected.

The RP-HPLC analysis proved that the purification process yielded efficient removal of the unreacted folic acid, which was in the final product below 0.3% mol.

Preparation & surface decoration of folate-targeted GNP

The GNP were synthesised by reduction of $HAuCl_4$ with citrate according to Turkevich's method [50]. Under the conditions selected, a red colloidal 3 nM GNP suspension was obtained. DLS and TEM analyses (Figure 3) showed that the production process yielded dimensionally homogenous particles. DLS analysis showed that the mean size of GNP was 14.6 ± 2.3 nm and the polydispersity index was 0.20 ± 0.08.

To endow GNP with biorecognition capacity and stealth features, the thiol ending functional polymers, namely the targeting FA-PEG-SH and the mPEG-SH (methoxy-PEG_{2kDa}-SH), were used for straightforward surface decoration [51]. Targeted GNP were obtained according to a two-step procedure. In the first step, GNP were decorated with FA-PEG-SH by incubation with a 50-fold FA-PEG-SH molar excess with respect to GNP. The particle surface was then saturated with mPEG-SH. Untargeted control particles (mPEG-GNP) were obtained by using only mPEG-SH for the coating.

Spectrophotometric analysis of particle coating efficiency showed that the decoration procedure yielded quantitative conjugation of FA-PEG-SH on the particle surface (98% conjugation efficiency), which corresponds to approximately 50 units of FA-PEG-SH per particle.

The saturation of the particle surface with 2 kDa mPEG-SH yielded a coating density of 0.92 PEG chains/nm^2 corresponding to about 650 PEG chains per particle. DLS analysis of FA-PEG-GNP (Figure 4A) showed that upon PEG coating, the size of the parti-

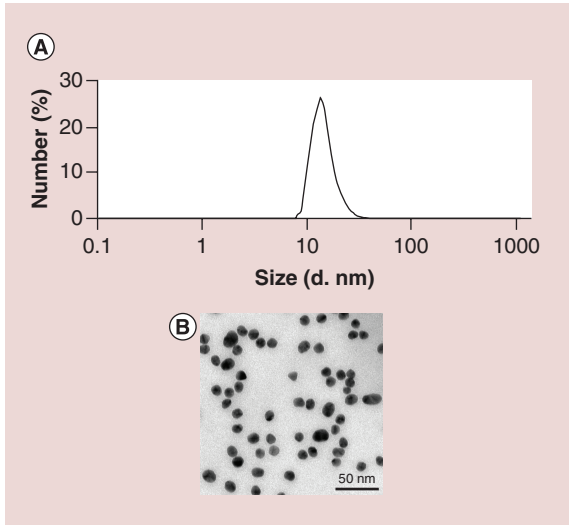

Figure 3. (A) Dynamic light scattering profile and (B) TEM image of gold nanoparticles covered with citrate corona.

cles increased from 14.6 ± 2.3 to 28.1 ± 5.2 nm. Notably, TEM imaging displayed a homogeneous coating corona surrounding the particles (Figure 4B) which was not present on the uncoated particles. UV-Vis spectroscopic analysis showed that the polymer coating resulted in a red shift of the maximum absorption from 520 to 523 nm (Figure 4C), which was attributed to the change in GNP surface features upon the replacement of the citrate corona with the polymers [52,53].

Cell uptake of folate-targeted GNP

The cell targeting capacity of GNP was investigated using three human cell lines that were selected for their different expression of folate receptor (FR): KB and HCT-116 cells over-express FR, whereas MCF7 cells do not over-express FR [54]. A preliminary flow cytometric assay (Figure 5) confirmed that MCF7 cells did not over-express FR (integrated mean fluorescence intensity, iMFI 0.72 ± 0.51), whereas HCT-116 and KB cells over-expressed FR at low (iMFI 16.84 ± 1.20, loFR) and high (iMFI 3309.04 ± 95.87, hiFR) density, respectively. MCF7 cells were thus selected as negative control.

A quantitative FA-PEG-GNP and mPEG-GNP uptake by the three cell lines either in the presence or absence of free FA was obtained using atomic absorption spectrometry (Figure 6).

Under the selected incubation conditions [55], about 19,800 and 2300 FA-PEG-GNP were found per KB

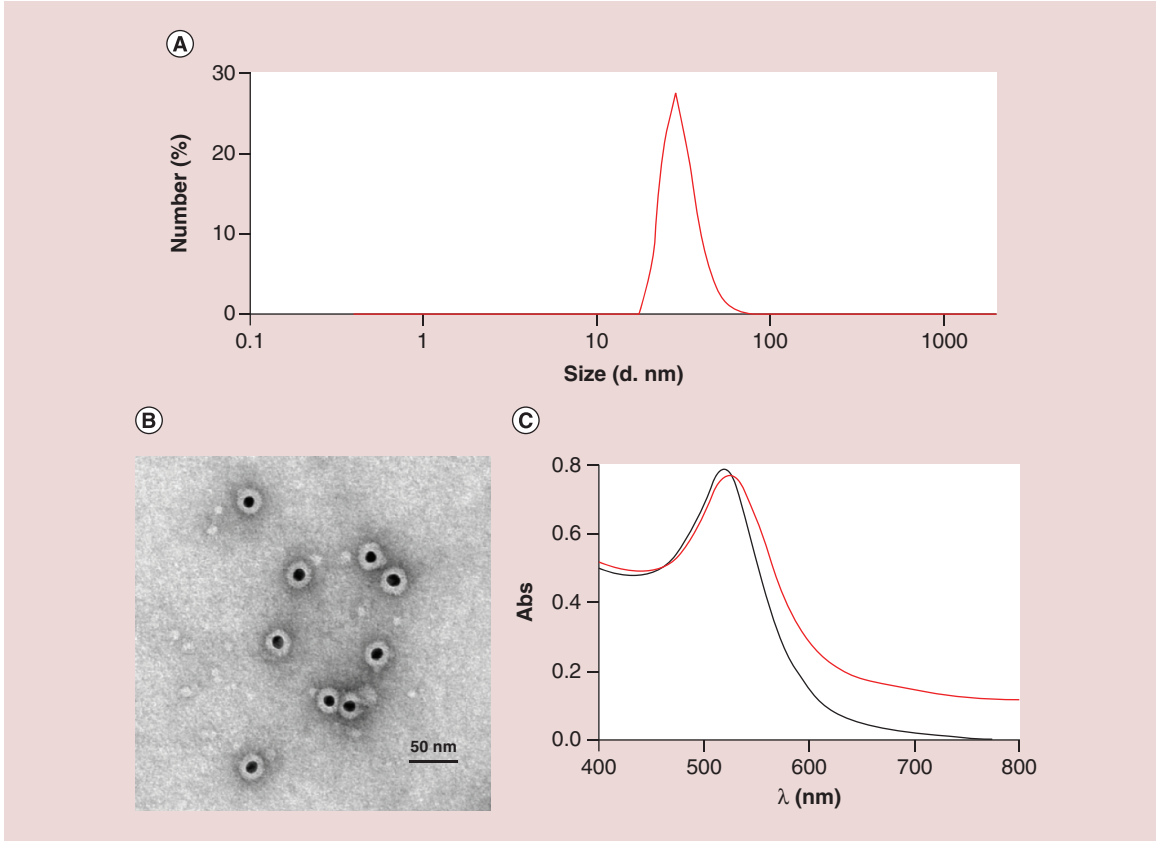

Figure 4. (A) Dynamic light scattering profile and (B) TEM image of FA-PEG-GNP. (C) UV-Vis spectrum of naked GNP (black line) and FA-PEG-GNP (red line) in deionized water.
FA-PEG-GNP: Folate-PEG decorated gold nanoparticles.

cell and HCT-116 cell, respectively, which corresponded to the different FR expression of the two cell lines. On the contrary, nontargeted particles (mPEG-GNP) showed a 36-times lower association with KB cells and 22-times lower association with HCT-116 cells compared with the targeted ones. The MCF7 cell uptake of the targeted particles was very low (570 particles per cell).

The cell competition assay performed by cell co-incubition with FA-PEG-GNP and free folic acid showed significant folate targeted GNP internalization inhibition in both KB and HCT-116 cells.

TEM images of KB cells incubated with FA-PEG-GNP showed that the particles were endocytosised by the cells and confined into intracellular vesicles that originate from the plasma membrane (Figure 7A & B). Notably, particles do neither undergo aggregation throughout the endocytic process nor clustering. On the contrary, control nontargeted GNP incubated with KB cells showed no intracellular uptake (Figure 7C & D).

Effects of folate-targeted GNP on cell proliferation upon US treatment

The efficacy and selectiveness of FA-PEG-GNP as sonosensitizers was investigated by evaluating their sonodynamic activity on MCF7, HCT-116 and KB cell lines (Figure 8).

Cell exposure to US alone, (US_n and US_t), did not affect the MCF7, HCT-116 and KB cell growth (Figure 8A–C). Similarly, no effect on cell growth was observed when cells were treated with both nontargeted (mPEG-GNP, data not shown) and targeted (FA-PEG-GNP) nanoparticles alone, without US exposure (Figure 8A–C). Combined FA-PEG-GNP/US treatment, with both US_n and US_t, led to significant decrease in HCT-116 and KB cell growth (Figure 8B & C). This did not occur in MCF7 cells (Figure 8A). Significant differences in the cytotoxicity were found when the loFR cells (HCT-116) incubated with FA-PEG-GNP were exposed to the two different US energy densities (US_n and US_t), with the US_t being the more efficient. Combined FA-PEG-GNP/US treatment induced significant decreases in cell growth of 30.18 ± 6.02%, 39.17 ± 5.81% and 55.65 ± 9.80% with US_n and 46.67 ± 5.03%, 69.35 ± 8.74% and 82.04 ± 8.03% with US_t at 24, 48 72 h, respectively, as compared with untreated cells (Figure 8B). On the contrary, US_n and US_t gave the same decrease in cancer cell growth at each time point in hiFR cells (KB) treated with FA-PEG-GNP (Figure 8C), in other words, 68.8 ± 7.09%, 78.29 ± 8.96% and 79.54 ± 8.37% with US_n and 67.77 ± 8.04%, 86.48 ± 9.15% and 92.63 ± 7.84% with US_t at 24, 48 and 72 h, respectively, compared with untreated cells (Figure 8C).

To further confirm the selective sonosensitizing activity of the FA-PEG-GNP under US exposure, a competition assay was performed by cell co-incubation with FA-PEG-GNP and free FA (200 μM) followed by US exposure. Notably, the cytotoxic activity of the sonodynamic treatment was completely suppressed both in HCT-116 (Figure 8D) and KB cells (Figure 8E).

Cell death study

The cell death mechanisms of HCT-116 and KB cells treated with FA-PEG-GNP/US were investigated by a flow cytometric assay. Since the percentages of apoptotic and necrotic cells at 2, 6 and 12 h do not show any significant differences, we herein report only the cell death analysis at 2 h after FA-PEG-GNP/US treatment to highlight the quick onset of cancer cell death (Figure 9). Cell death of HCT-116 and KB cells sonodynamically treated was found to occur with a significant increase ($p < 0.001$) in the percentages of late apoptotic/necrotic cells (Figure 9A & B). Furthermore, the FA-PEG-GNP sonoactivation with US_t induced a higher increase ($p < 0.01$) in the percentages of early apoptotic cells in KB (Figure 9B) as compared with HCT-116 cells (Figure 9A).

Intracellular ROS assessment upon folate-targeted GNP incubation & US exposure

Since the mechanism underlying chemical sensitizer cytotoxicity upon US exposure is thought to be ROS generation [9], it was decided to evaluate ROS production after each treatment type. Cell incubation with FA-PEG-GNP without US activation did not induce

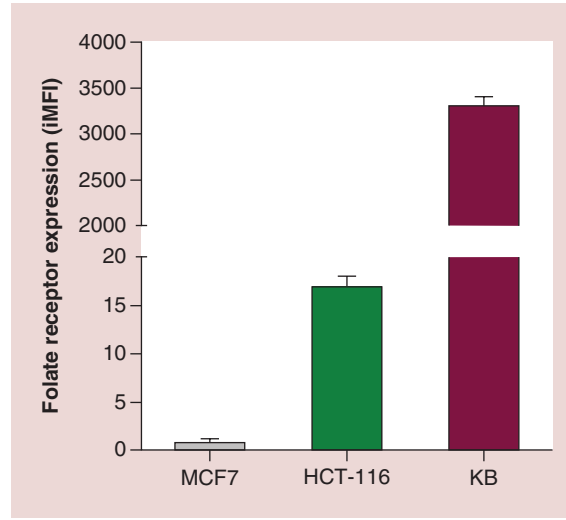

Figure 5. Folate receptor expression of MCF7, HCT-116 and KB cells by flow cytometry. Data are expressed as iMFI, defined as the percentage of FR-positive cells multiplied by mean fluorescence intensity of FR-positive cells.
FR: Folate receptor; iMFI: Integrated mean fluorescence intensity.

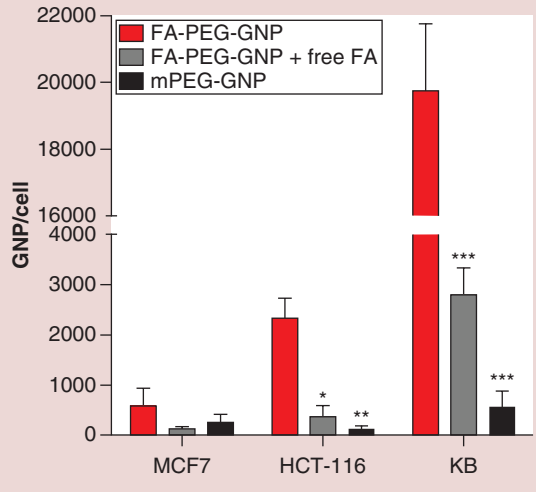

Figure 6. Cell uptake profile of folate targeted (folate-PEG decorated gold nanoparticles) and nontargeted (mPEG-GNP) gold nanoparticles by MCF7, HCT-116 and KB cell lines. Folate-targeted GNP were also incubated with cells in the presence of free FA as competitive agent. Statistical significance was calculated versus folate targeted particle uptake tested on each cell line: *$p < 0.05$, **$p < 0.01$, ***$p < 0.001$.
GNP: Gold nanoparticles.

an intracellular increase in ROS production in either cell line HCT-116 or KB (Figure 10). Cell exposure to US alone, in absence of FA-PEG-GNP, induced a very limited increase in ROS production at both US energy densities (Figure 10). The sonodynamic treatment of cells incubated with FA-PEG-GNP at both energy densities induced a significant increase in ROS production (Figure 10). The highest level of intracellular ROS was achieved 15 min after the exposure of HCT-116 cells to US_n (Figure 10A) and 1 min after the exposure of KB cells to US_t (Figure 10B). A less intense and delayed pattern of ROS generation was found in the loFR HCT-116 cells (Figure 10A), and a more intense and faster ROS generation pattern was shown by the hiFR KB cells (Figure 10B).

A ROS scavenging assay with N-acetylcysteine (NAC) was carried out to clarify the correlation between intracellular ROS production and the cancer cell death induced by FA-PEG-GNP/US treatment. Interestingly, NAC suppressed ROS production and cytotoxicity only when FA-PEG-GNP treated HCT-116 cells were sonoactivated with the lower US energy density US (Figure 11A & C). When these cells were treated with the higher US energy density, a remarkable decrease of cancer cell growth, as compared with untreated cells, was only observed after 72 h (43.73 ± 8.2%; Figure 11A). This was accompanied by a slight but significant increase in ROS production 1 min after US exposure (Figure 11C). On the other hand, in KB cells NAC was not able to sup-

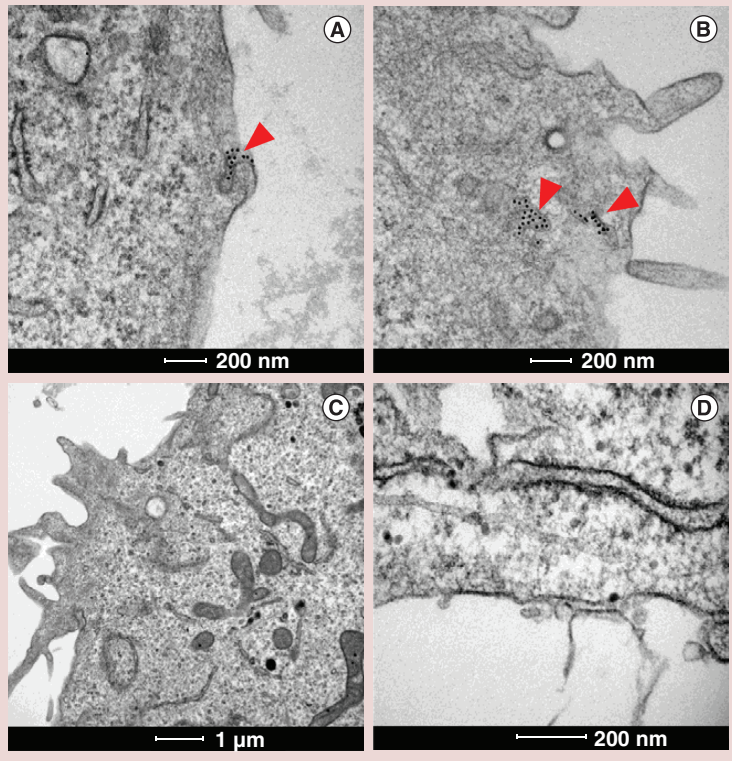

Figure 7. (A & B) TEM images of KB cells incubated with folate targeted gold nanoparticles and (C & D) nontargeted gold nanoparticles. Red arrows indicate gold nanoparticles.

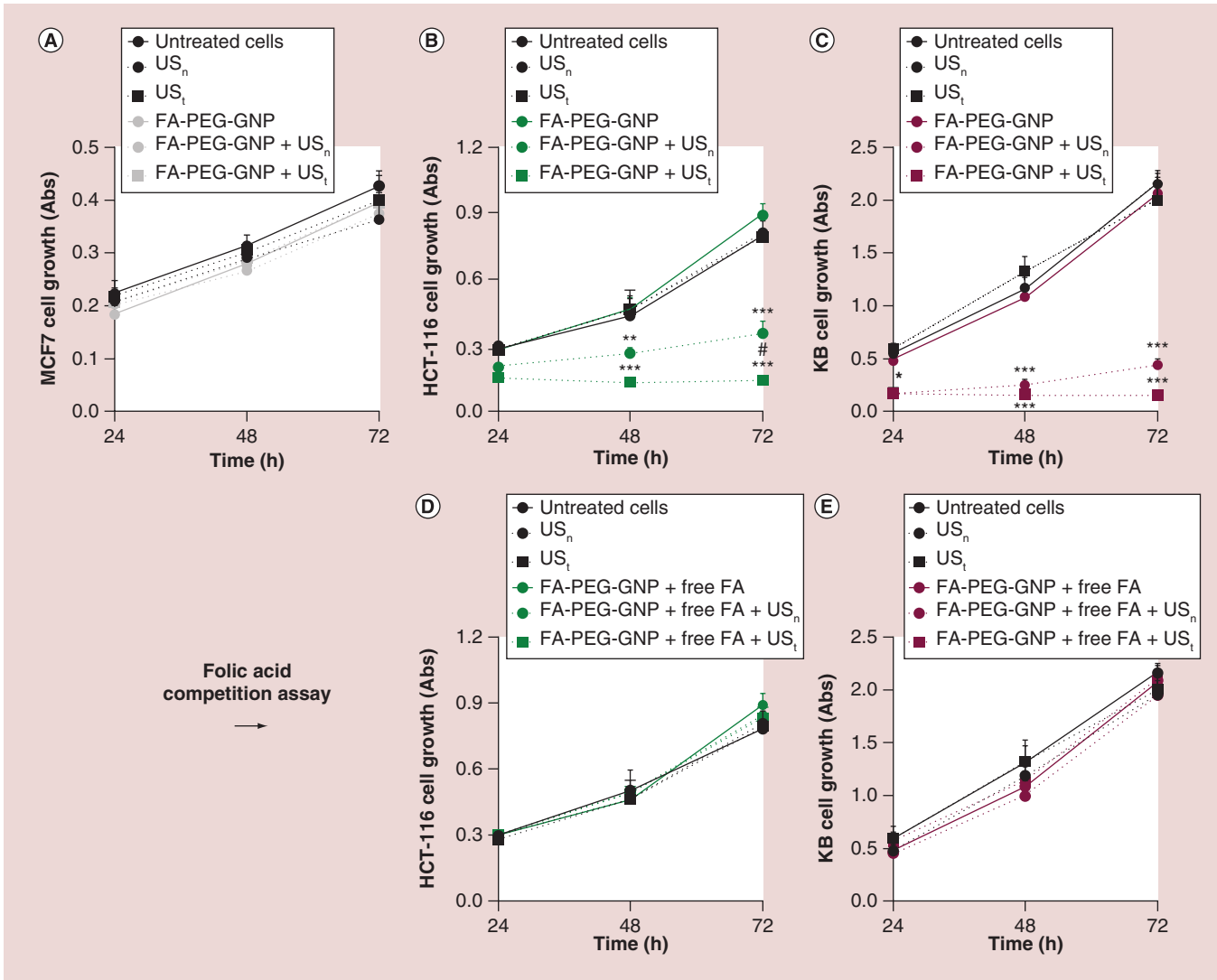

Figure 8. Effect of folate-PEG decorated gold nanoparticles upon irradiation with ultrasound on cell lines with differing folate receptor expression. Cells were exposed for 2 h to 1 nM folate-PEG decorated gold nanoparticle (FA-PEG-GNP) and ultrasound (US) irradiation was carried out for 5 min at two different energy densities (US_n: 0.008 mJ/cm^2 and US_t: 0.080 mJ/cm^2). The upper panels show the effect of US alone (both US_n and US_t, black lines), of FA-PEG-GNP alone and of FA-PEG-GNP irradiated by US (both US_n and US_t) on MCF7 (A, gray lines), HCT-116 (B, green lines) and KB (C, purple lines) cell growth. The lower panels report the effect of US alone (both US_n and US_t, black lines), of FA-PEG-GNP alone and of FA-PEG-GNP irradiated by US (both US_n and US_t) on HCT-116 (D, green lines) and KB (E, purple lines) cell growth with 200 μM free FA added to the culture medium to evaluate the receptor mediated uptake selectivity of FA-PEG-GNP. Statistically significant difference versus untreated cells: *$p < 0.05$; **$p < 0.01$; ***$p < 0.001$ and between US_n and US_t treatment: #$p < 0.05$.

press either ROS generation or US-triggered FA-PEG-GNP cytotoxicity at either energy density (Figure 11B). Notably, the amount of ROS generated by the FA-PEG-GNP/US_t treatment, which caused a moderate increase of the medium temperature, at 1 min (Figure 11D) was equivalent to levels detected in the absence of the ROS scavenging agent (Figure 10B).

Discussion

Improvements in therapeutic activity and selectivity are the major goals in the development of any innovative anticancer treatment. Many approaches have been introduced to achieve these goals and most of them have been based on drug delivery [56,57]. However, combined strategies have recently attracted increasing levels of interest [58–60] and among them SDT has the potential to open up novel frontiers in cancer treatment.

Despite SDT's promising features, the poor reproducibility of treatment outcomes and inadequate correlation between in vitro and the in vivo results have hampered the development of this robust treatment

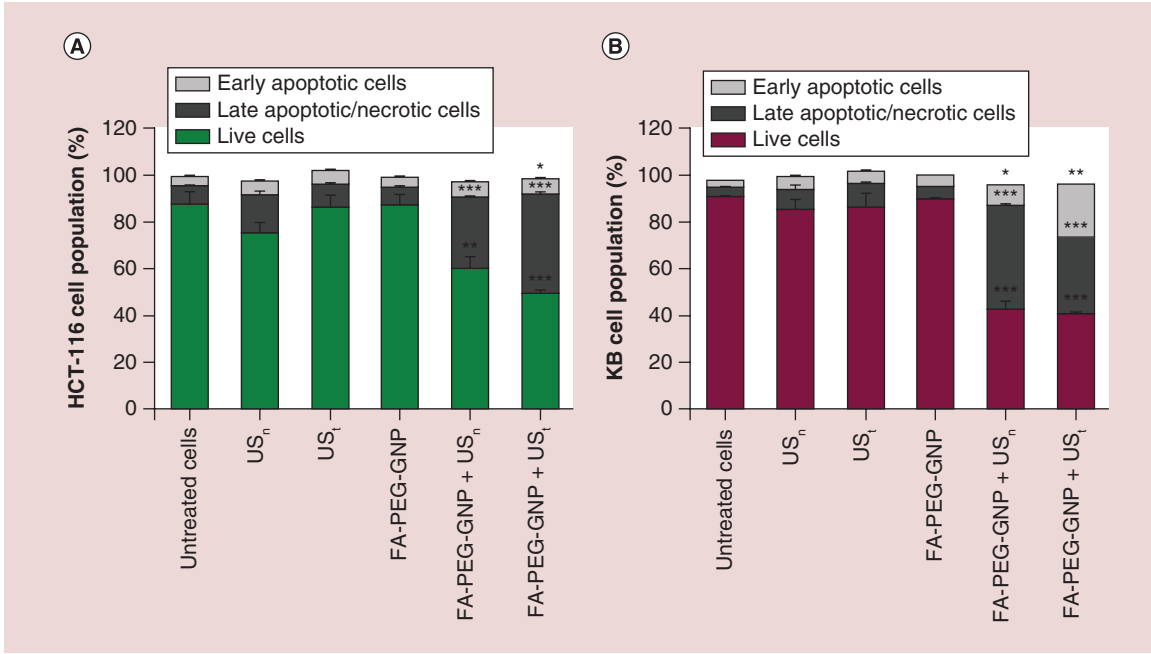

Figure 9. Cell death induced by folate-PEG decorated gold nanoparticle irradiated with ultrasound. HCT-116 (A) and KB (B) cells were exposed for 2 h to 1 nM FA-PEG-GNP and ultrasound (US) irradiation was carried out for 5 min at two different energy densities (US_n: 0.008 mJ/cm^2 and US_t: 0.080 mJ/cm^2). Cells were stained with APC-Annexin V and Sytox® Green 2 h after the different treatment types and analyzed by flow cytometry to quantify the viable cells (negative to APC-Annexin V and Sytox Green), early apoptotic cells (positive to APC-Annexin V and negative to Sytox Green), and late apoptotic/necrotic cells (positive to Annexin V and Sytox Green). Statistically significant difference versus untreated cells: *$p < 0.05$; **$p < 0.01$; ***$p < 0.001$.
FA-PEG-GNP: Folate-PEG decorated gold nanoparticle.

protocol, slowing its translation to clinical practice [61]. The development of innovative sonosensitizers is therefore paramount if we are to overcome these drawbacks and boost the effect of US and while taking advantage of the combined effects of possible sonoluminescence emitted by US exposure.

According to this hypothesis, US sensitive nanoparticles were designed in order to achieve accumulation in solid tumors by passive mechanisms and be internalized into cancer cells by active mechanisms. Therefore, GNPs were sized to exploit the enhanced tumor permeability and retention effect and surface decorated to achieve the active targeting of cancer cells and cell internalization. The combination of these features with focused US treatment can provide for enhanced spatially controlled sonosensitizing effects.

As a proof of concept, GNP were decorated with folic acid (FA-PEG-GNP) to bestow selectivity for cancer cells that over-express the folate receptor. Folic acid was conjugated to the particle suface via a PEG spacer, which guarantees the exposure and flexibility of the biological ligand. This directly results in efficient receptor mediated uptake by folate receptor expressing cancer cells. The selection of the targeting agent density was based on our previous studies showing that an average of 50 folate units per particle yielded suitable folate receptor biorecognition and high cell uptake efficiency of targeted GNP [55].

The surface saturation of the FA-PEG-SH decorated nanoparticles with mPEG-SH was pursued to endow the particles with stealth properties while ensuring exposure of the targeting agent at the tip of the 3.5 kDa FA-PEG-SH chains. mPEG was found to enhance the colloidal stability of the particles and inhibit GNP aggregation as observed by intracellular TEM imaging, whereas did not prevent the FR recognition. The targeted particles were in fact efficiently taken up by FR overexpressing cancer cells and limitately internalized by the control cell line (MCF7) which does not overexpress the FR. Selective recognition and cell uptake was confirmed by competition study with free folic acid, in which particle uptake was inhibited in HCT-116 and KB cells. Furthermore, the extent of particle association to cells was affected by the cell expression level of the FR, being higher in hiFR KB cells and lower in loFR HCT-116 cells. To note that the nontargeted control GNP (mPEG-GNP) were barely detected in the cytosol of all cell lines by intracellular TEM imaging, which is probably due to negligible mPEG-GNP diffusion across cell membranes in agreement with previous studies reported by Kanaras et al. [53].

The selective cytotoxicity of the combined FA-PEG-GNP/US treatment has been demonstrated by using cells with different degree of FR expression and by competitive studies.

Cytotoxicity studies showed that the sonoactivation of FA-PEG-GNP was ineffective in the case of cells that did not over-express the FR, namely MCF7. On the contrary, FA-PEG-GNP provide significant cancer cell sensitization to US which in turn yields selective and remarkable cytotoxicity in FR overexpressing HCT-116 and KB cells. This cytotoxic effect was suppressed when free folic acid was co-incubated with FA-PEG-GNP, demonstrating that the targeted nanoparticle cell uptake is paramount to the overall efficacy of the treatment. Thus, we can conclude that the synergistic effect between targeted GNP and US-induced acoustic cavitation occurs upon particle endocytosis.

In the literature it is reported that the success of the folic acid-targeted therapeutic system normally relies on the level of FR overexpression for a given tumor; low FR overexpressing cancers were found to have limited response to folate-targeted therapies [29,62]. Nevertheless, the cytotoxicity results obtained on MCF7, HCT-116 and KB cells demonstrate the high selectivity of FA-PEG-GNP/US treatment for all FR overexpressing cells. It is worth to note that the US-activated FA-PEG-GNP efficiently induced significant cell death in cells with low and high levels of FR

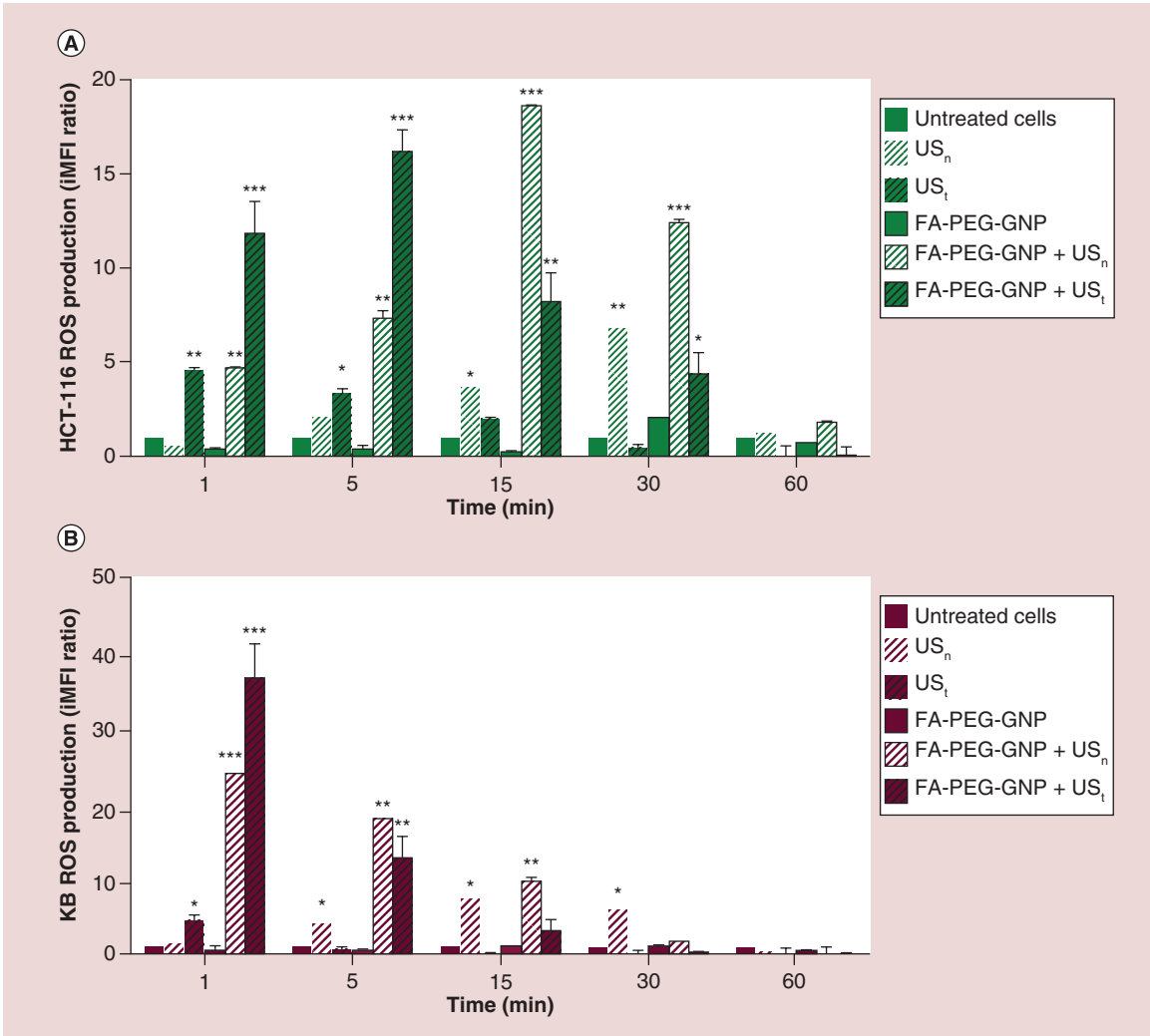

Figure 10. ROS production induced by folate-PEG decorated gold nanoparticle irradiation with ultrasound.
HCT-116 (A) and KB (B) cells were exposed for 2 h to 1 nM FA-PEG-GNP and ultrasound (US) exposure was carried out for 5 min at at two different energy densities (US_n: 0.008 mJ/cm^2 and US_t: 0.080 mJ/cm^2). ROS production after the different treatment types was quantified according to the dichlorofluorescin-diacetate assay with flow cytometry and expressed as iMFI ratio to yield the ratiometric increase in fluorescence per time point. Statistically significant difference versus untreated cells: *$p < 0.05$; **$p < 0.01$; ***$p < 0.001$.
FA-PEG-GNP: Folate-PEG decorated gold nanoparticle; iMFI: integrated mean fluorescence intensity.

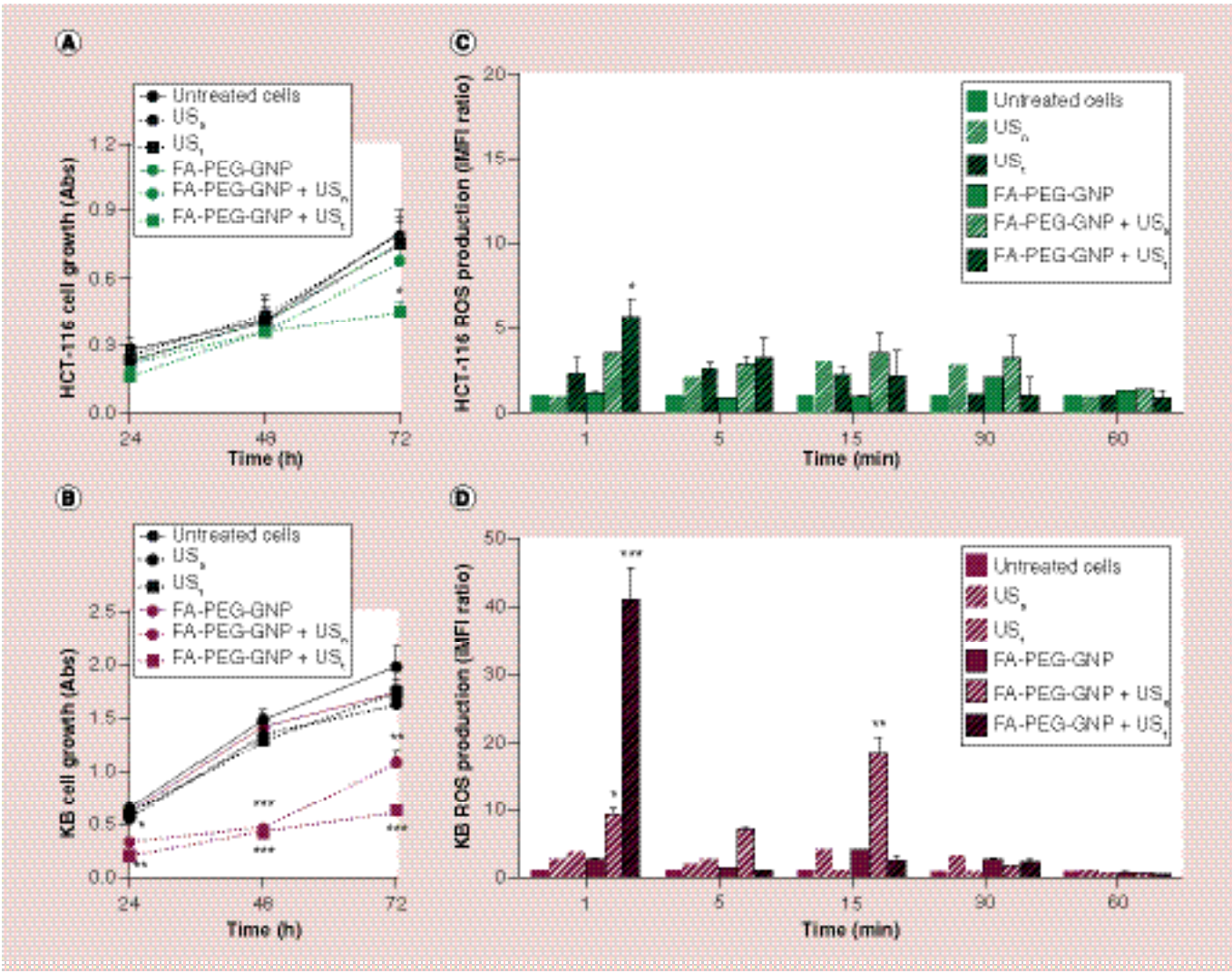

Figure 11. Effect of the reactive oxygen species scavenging agent, N-acetylcysteine, on cell proliferation and reactive oxygen species production as induced by folate-PEG decorated gold nanoparticle's irradiation with ultrasound. HCT-116 (A & C) and KB (B & D) cells were exposed for 2 h to 1 nM folate-PEG decorated gold nanoparticle (FA-PEG-GNP) with the addition of 5.0 mM N-acetylcysteine (NAC) to the culture medium and ultrasound (US) exposure was carried out for 5 min at two different energy densities (US_n: 0.008 mJ/cm^2 and US_t: 0.080 mJ/cm^2). The left panels (A & B) report the effect of FA-PEG-GNP irradiation with US (both US_n and US_t), of US alone (both US_n and US_t) and of FA-PEG-GNP alone in the presence of the reactive oxygen species (ROS) scavenging agent, NAC. The right panels (C & D) report the ROS production of FA-PEG-GNP irradiated with US (both US_n and US_t), of US alone (both US_n and US_t) and of FA-PEG-GNP alone in the presence of the ROS scavenging agent, NAC. Statistically significant difference versus untreated cells: *$p < 0.05$; **$p < 0.01$; ***$p < 0.001$.
FA-PEG-GNP: Folate-PEG decorated gold nanoparticle.

overexpression. This sonoactivation process would therefore seem to be effective on a wide range of cancers, which include low and high FR overexpressing cells. Interestingly, despite loFR cells (HCT-116) have a 8.6-times lower targeted GNP uptake with respect to hiFR cells (KB), their response to the combined treatment with US_n and US_t is not so different, and this may be due to a higher HCT-116 cell sensitivity to US-induced ROS. These results suggest that the cytotoxicity induced by the sonoactiovation of FA-PEG-GNP therefore does not only depend on the degree of FR overexpression, but also on the intrinsic cell sensitivity to the treatment outcomes, namely ROS [63].

The studies undertaken to elucidate the mechanism of cancer cell death induced by FA-PEG-GNP/US treatment showed that incubation with FA-PEG-GNP and exposure to US_n or US_t provoked a sudden occurrence of necrotic rather than apoptotic cell death. When looking at the intracellular ROS production of the two cell lines that over-express FR and the two energy density exposures, different behaviors

were observed. The higher intracellular ROS generation detected in hiFR KB cells may be ascribed to the higher amount of particle uptake compared with loFR HCT-116 cells (Figure 6). In the case of KB cells, ROS production was not found to depend on US energy density. On the contrary, the rate and level of intracellular ROS production in the loFR cell line was more rapid and higher in level at the highest energy density (US_t). These results suggest, as expected, that ROS production depends on both intracellular particle density and US intensity. In the case of high FA-PEG-GNP cell uptake obtained with KB cells, the effect of US energy density is negligeable, while in the case of low FA-PEG-GNP cell uptake observed in HCT-116 cells the US energy density is critical to the citotoxicty.

The ROS scavenger NAC was used in order to provide additional information about the involvement of ROS in cell death upon the sonodynamic activation of intracellular FA-PEG-GNP. Interestingly, the effect of NAC was found to depend on both cell line and US energy density. NAC prevented HCT-116 cell death, supporting the hypothesis that the cytotoxicity was mainly ascribable to the ROS production. This hypothesis was further confirmed by the results obtained with KB cells, which endocytosed high amounts of FA-PEG-GNP. In this case, in fact the NAC effect could not be observed when the sonoactivation was performed with the higher US intensity because, under this condition, the ROS production was very high. On the contrary, when sonoactivation was perfomed with the lower US intensity, that produced a not so high level of ROS, NAC efficiently suppressed intracellular ROS generation and cytotoxicity.

One mechanistic explanation of the effects that are induced upon GNP US-exposure is that ROS production might also be a consequence of the GNP SPR effect. Accordingly, US-induced cavitation can generate light that is absorbed by GNP and quickly converted to heat which induces ROS production and cancer cell death. This hypothesis appears to be in line with observations made by Sazgarnia et al.[64]. Indeed, these authors investigated sonoluminescence on agel phantom containing GNP loaded with propoprophyrin IX. They highlighted the occurrence of gas bubbles, transient cavitation upon US irradiation, the collapse of the bubbles, sonoluminescence and free radical generation. Moreover, Wang et al. [65] developed a GNP coated mesoporous silica nanocapsule-based platform that, under the guidance of intensified US imaging, was able to enhance high intensity focused ultrasound ablation efficacy on rabbit xenograft tumors. Other metal nanoparticles, such as silver [66] or zinc oxide [67] nanoparticles, may also be potentially suitable for use as nanosonosensitizers due to their inherent ability to absorb luminescence irradiation. However, GNP show several beneficial properties, such as the ability to behave as localized thermal loaders[68] and theranostic agents[69], while they also possess a non toxic and biocompatible metal core[25,70], making them an intriguing platform for the development of the next generation of nanosonosensitizers.

Conclusion

The ability of US to activate the targeted GNP for cancer cell killing in FR overexpressing cell lines confirmed the hypotheses published by Wen et al.[71] that the combination of GNP and US may be a promising strategy for future medical applications. To the

Executive summary

- Folate-PEG decorated gold nanoparticles (FA-PEG-GNP) have been designed to target folate receptor overexpressing human cancer cells.
- The GNP were generated by reduction of chloroauric acid and coated with a folate-$PEG_{3.5kDa}$-SH (FA-PEG-SH) at a density of 50 FA-PEG-SH units per particle and then surface saturated with methoxy-PEG-SH (mPEG-SH).
- In vitro experiments performed on folate receptor overexpressing (KB and HCT-116) and non overexpressing (MCF7) human cancer cells showed that the particle association to the cells correlated to the folate receptor expression.
- Competition cell uptake assays performed in the presence of folic acid confirmed that FA-PEG-GNP selectively targeted KB and HCT-116 cells.
- A selective killing of cancer cells with a peculiar signature (namely overexpression of a selected receptor) was achieved by cancer cell incubation with targeted GNPs and exposure to two different ultrasound energy densities.
- The combined approach of targeted GNP and ultrasound exposure was able to determine a remarkable reactive oxygen species (ROS) generation and increase in necrotic cancer cells, compared with control conditions.
- When KB and HCT-116 cells were treated with FA-PEG-GNP at the lower US energy density, N-acetylcysteine, used as ROS scavenger, completely suppressed ROS production and cytototoxicity.
- This is the first work that demonstrates how cancer targeted GNP can act as ultrasound sensitizers by themselves paving the way to a promising strategy for the site-specific treatment of cancer.

best of our knowledge, our study demonstrates for the first time the role of targeted GNP as sonosensitizers. Indeed, the results reported here concerning targeted GNP for sonodynamic treatment showed a remarkable decrease in cancer cell growth at different US treatment conditions (US_n and US_t).

In conclusion, targeting GNP have proven themselves to be effective sonosensitizers for the US-based treatment of cancer paving the way to novel approach in selective cancer treatments.

Acknowledgements

The authors would like to thank Prof. MNV Ravi Kumar for inspiring their collaboration and Dr D Lawson for his critical proofreading and advice.

Financial & competing interests disclosure

This work was financially supported by Associazione Italiana per la Ricerca sul Cancro (grant MFAG-2012, MFAG-13048), by University of Torino (grant "Ricerca Locale 2015") and by University of Padova (grant "Progetto di Ricerca di Ateneo" CPDA121714, CUP C94H12000020005 and grant "Progetto strategico di ateneo – Bando 2011" C98C13002740005, PROT. STPD11RYPT_02). The authors have no other relevant affiliations or financial involvement with any organization or entity with a financial interest in or financial conflict with the subject matter or materials discussed in the manuscript apart from those disclosed.

No writing assistance was utilized in the production of this manuscript.

References

Papers of special note have been highlighted as: • of interest; •• of considerable interest

1 Frenkel V. Ultrasound mediated delivery of drugs and genes to solid tumors. Adv. Drug Deliv. Rev. 60(10), 1193–1208 (2008).

•• An important review on the most important ultrasound mechanisms that can be employed for therapeutic applications against solid tumors.

2 Leighton TG. What is ultrasound? Prog. Biophys. Mol. Biol. 93(1–3), 3–83 (2007).

3 Kennedy JE. High-intensity focused ultrasound in the treatment of solid tumours. Nat. Rev. Cancer 5(4), 321–327 (2005).

4 Mchale AP, Callan JF, Nomikou N, Fowley C, Callan B. Sonodynamic therapy: concept, mechanism and application to cancer treatment. Adv. Exp. Med. Biol. 880, 429–450 (2016).

5 Suslick KS, Flannigan DJ. Inside a collapsing bubble: sonoluminescence and the conditions during cavitation. Annu. Rev. Phys. Chem. 59, 659–683 (2008).

6 Vazquez G, Camara C, Putterman S, Weninger K. Sonoluminescence: nature's smallest blackbody. Opt. Lett. 26(9), 575–577 (2001).

7 Tachibana K, Feril LB, Jr., Ikeda-Dantsuji Y. Sonodynamic therapy. Ultrasonics 48(4), 253–259 (2008).

8 Umemura S, Yumita N, Nishigaki R, Umemura K. Mechanism of cell damage by ultrasound in combination with hematoporphyrin. Jpn J. Cancer Res. 81(9), 962–966 (1990).

9 Misik V, Riesz P. Free radical intermediates in sonodynamic therapy. Ann. NY Acad. Sci. 899, 335–348 (2000).

10 Dolmans DE, Fukumura D, Jain RK. Photodynamic therapy for cancer. Nat. Rev. Cancer 3(5), 380–387 (2003).

11 Agostinis P, Berg K, Cengel KA et al. Photodynamic therapy of cancer: an update. CA Cancer J. Clin. 61(4), 250–281 (2011).

12 Canaparo R, Varchi G, Ballestri M et al. Polymeric nanoparticles enhance the sonodynamic activity of meso-tetrakis (4-sulfonatophenyl) porphyrin in an in vitro neuroblastoma model. Int. J. Nanomedicine 8, 4247–4263 (2013).

13 Meng Y, Zou C, Madiyalakan R et al. Water-soluble and biocompatible sono/photosensitizer nanoparticles for enhanced cancer therapy. Nanomedicine (Lond.) 5(10), 1559–1569 (2010).

14 Sazgarnia A, Shanei A, Meibodi NT, Eshghi H, Nassirli H. A novel nanosonosensitizer for sonodynamic therapy: in vivo study on a colon tumor model. J. Ultrasound Med. 30(10), 1321–1329 (2011).

15 Kharin A SO, Geloen a, Alekseev S, Rogov A, Lysenko V, Timoshenko V. Carbon fluoroxide nanoparticles as fluorescent labels and sonosensitizers for theranostic applications. Sci. Technol. Adv. Mater. 16(4), 6 (2015).

16 Yumita N, Iwase Y, Imaizumi T et al. Sonodynamically-induced anticancer effects by functionalized fullerenes. Anticancer Res. 33(8), 3145–3151 (2013).

17 Osminkina LA NaL, Sviridov AP, Andronova NV et al. Porous silicon nanoparticles as efficient sensitizers for sonodynamic therapy of cancer. Microporous Mesoporous Mat. 210, 7 (2015).

18 Osminkina LA, Sivakov VA, Mysov GA et al. Nanoparticles prepared from porous silicon nanowires for bio-imaging and sonodynamic therapy. Nanoscale Res. Lett. 9(1), 463 (2014).

19 Sviridov AP AVG, Ivanoca EM, Osminkina LA, Tamarov KP, Timoshenko VYu. Porous silicon nanoparticles as sensitizers for ultrasonic hyperthermia. Appl. Phys. Lett. 103(19), 4 (2013).

20 Harada Y, Ogawa K, Irie Y et al. Ultrasound activation of TiO2 in melanoma tumors. J. Control. Release 149(2), 190–195 (2011).

21 Ninomiya K, Noda K, Ogino C, Kuroda S, Shimizu N. Enhanced OH radical generation by dual-frequency ultrasound with TiO2 nanoparticles: its application to targeted sonodynamic therapy. Ultrason. Sonochem. 21(1), 289–294 (2014).

22 You DG, Deepagan VG, Um W et al. ROS-generating TiO_2 nanoparticles for non-invasive sonodynamic therapy of cancer. Sci. Rep. 6, 6 (2016).

23 Libutti SK, Paciotti GF, Byrnes AA et al. Phase I and pharmacokinetic studies of CYT-6091, a novel PEGylated colloidal gold-rhTNF nanomedicine. Clin. Cancer Res. 16(24), 6139–6149 (2010).

•• Describes one of the most relevant clinical studies involving gold nanoparticles (GNP) for anticancer therapy.

24 Kim BY, Rutka JT, Chan WC. Nanomedicine. N. Engl. J. Med. 363(25), 2434–2443 (2010).

25 Khlebtsov N, Dykman L. Biodistribution and toxicity of engineered gold nanoparticles: a review of in vitro and in vivo studies. Chem. Soc. Rev. 40(3), 1647–1671 (2011).

•• Reviews the recent results concerning biosafety of GNP and offers a useful background for GNP design.

26 Huang X E-SM. Gold nanoparticles: optical properties and implementations in cancer diagnosis and photothermal therapy. J. Adv. Res. 1, 13–28 (2010).

27 Link S E-SM. Shape and size dependence of radiative, non-radiative and photothermal properties of gold nanocrystals. Int. Rev. Phys. Chem. 19(3), 409–453 (2000).

28 Kennedy LC, Bickford LR, Lewinski NA et al. A new era for cancer treatment: gold-nanoparticle-mediated thermal therapies. Small 7(2), 169–183 (2011).

29 Bazak R, Houri M, El Achy S, Kamel S, Refaat T. Cancer active targeting by nanoparticles: a comprehensive review of literature. J. Cancer Res. Clin. Oncol. 141(5), 769–784 (2015).

• Reviews the requirements, risks and pros of using targeted nanocarriers to enhance the drug efficacy.

30 Mehra NK, Mishra V, Jain NK. Receptor-based targeting of therapeutics. Ther. Deliv. 4(3), 369–394 (2013).

31 Mansoori GA, Brandenburg KS, Shakeri-Zadeh A. A comparative study of two folate-conjugated gold nanoparticles for cancer nanotechnology applications. Cancers (Basel) 2(4), 1911–1928 (2010).

32 Feng D, Song Y, Shi W, Li X, Ma H. Distinguishing folate-receptor-positive cells from folate-receptor-negative cells using a fluorescence off-on nanoprobe. Anal. Chem. 85(13), 6530–6535 (2013).

33 Krystofiak ES MV, Steeber DA, Oliver JA. Elimination of tumor cells using folate receptor targeting by antibody-conjugated, gold-coated magnetite nanoparticles in a murine breast cancer model. J. Nanomater. 2012, 1–9 (2012).

34 Salmaso S, Caliceti P. Stealth properties to improve therapeutic efficacy of drug nanocarriers. J. Drug Deliv. 2013, 374252 (2013).

35 De Jong WH, Hagens WI, Krystek P, Burger MC, Sips AJ, Geertsma RE. Particle size-dependent organ distribution of gold nanoparticles after intravenous administration. Biomaterials 29(12), 1912–1919 (2008).

36 Longmire M, Choyke PL, Kobayashi H. Clearance properties of nano-sized particles and molecules as imaging agents: considerations and caveats. Nanomedicine (Lond.) 3(5), 703–717 (2008).

37 Oh N, Park JH. Endocytosis and exocytosis of nanoparticles in mammalian cells. Int. J. Nanomedicine 9(Suppl. 1), 51–63 (2014).

38 Bartczak D, Nitti S, Millar TM, Kanaras AG. Exocytosis of peptide functionalized gold nanoparticles in endothelial cells. Nanoscale 4(15), 4470–4472 (2012).

39 Chithrani BD, Chan WC. Elucidating the mechanism of cellular uptake and removal of protein-coated gold nanoparticles of different sizes and shapes. Nano Lett. 7(6), 1542–1550 (2007).

40 Sims GE, Snape TJ. A method for the estimation of polyethylene glycol in plasma protein fractions. Anal. Biochem. 107(1), 60–63 (1980).

41 Kranz DM, Patrick TA, Brigle KE, Spinella MJ, Roy EJ. Conjugates of folate and anti-T-cell-receptor antibodies specifically target folate-receptor-positive tumor cells for lysis. Proc. Natl Acad. Sci. USA 92(20), 9057–9061 (1995).

42 Riddles PW, Blakeley RL, Zerner B. Ellman's reagent: 5,5′-dithiobis(2-nitrobenzoic acid)–a reexamination. Anal. Biochem. 94(1), 75–81 (1979).

43 Turkevich P SP, Hillier J. The formation of colloidal gold. J. Phys. Chem. 57(7), 670–673 (1953).

44 Liu X, Atwater M, Wang J, Huo Q. Extinction coefficient of gold nanoparticles with different sizes and different capping ligands. Colloids Surf. B. Biointerfaces 58(1), 3–7 (2007).

45 Jain Pk LK, El-Sayed Ih, El-Sayed Ma. Calculated absorption and scattering properties of gold nanoparticles of different size, shape, and composition: applications in biological imaging and biomedicine. J. Phys. Chem. B 110(14), 7238–7248 (2006).

46 Link S E-SM. Spectral properties and relaxation dynamics of surface plasmon oscillations in gold and silver nanodots and nonorods. J. Phys. Chem. B 103(40), 8410–8426 (1999).

47 Gallon E, Matini T, Sasso L et al. Triblock copolymer nanovesicles for pH-responsive targeted delivery and controlled release of siRNA to cancer cells. Biomacromolecules 16(7), 1924–1937 (2015).

• Describes for the first time an alternative 'whole cell' method for phenotyping of folate receptor expressing cancer cells accounting for only the membrane-associated receptor.

48 Durando G GC, Canaparo R, Serpe L. Acoustic characterization of ultrasound fields able to induce sonodynamic activity in an in vitro cancer model. In: 2015 IEEE International Symposium on Medical Measurements and Applications, MeMeA 2015 – Proceedings. The Institute of Electrical and Electronics Engineers, 121–124 (2015).

49 Matini T FN, Battocchio A, Spain Sg et al. Synthesis and characterization of variable conformation pH responsive block copolymers for nucleic acid delivery and targeted cell entry. Polym. Chem. 5(5), 1626–1636 (2014).

50 Turkevich P SP, Hillier J. A study of the nucleation and growth processes in the synthesis of colloidal gold. Discuss. Faraday Soc. 11, 55–75 (1951).

51 Dreaden EC, Austin LA, Mackey MA, El-Sayed MA. Size matters: gold nanoparticles in targeted cancer drug delivery. Ther. Deliv. 3(4), 457–478 (2012).

52 Chuang Mk CF, Hsu Cs. Gold nanoparticle-graphene oxide nanocomposites that enhance the device performance of polymer solar cells. J. Nanomater. 2014, 736879 (2014).

53 Kanaras AG, Kamounah FS, Schaumburg K, Kiely CJ, Brust M. Thioalkylated tetraethylene glycol: a new ligand for water soluble monolayer protected gold clusters. Chem. Commun. (Camb.) (20), 2294–2295 (2002).

54 Chen H, Ahn R, Van Den Bossche J, Thompson DH, O'Halloran TV. Folate-mediated intracellular drug delivery increases the anticancer efficacy of nanoparticulate formulation of arsenic trioxide. Mol. Cancer Ther. 8(7), 1955–1963 (2009).

55 Mastrotto F, Caliceti P, Amendola V et al. Polymer control of ligand display on gold nanoparticles for multimodal switchable cell targeting. Chem. Commun. (Camb.) 47(35), 9846–9848 (2011).

56 Swain S, Babu SM, Beg S, Jena J. Nanoparticles for cancer targeting: current and future directions. Curr. Drug Deliv. doi:10.2174/1567201813666160713121122 (2016) (Epub ahead of print).

57 Xu X, Ho W, Zhang X, Bertrand N, Farokhzad O. Cancer nanomedicine: from targeted delivery to combination therapy. Trends Mol. Med. 21(4), 223–232 (2015).

58 Obaid G, Broekgaarden M, Bulin AL et al. Photonanomedicine: a convergence of photodynamic therapy and nanotechnology. Nanoscale 8(25), 12471–12503 (2016).

59 Qian X, Zheng Y, Chen Y. Micro/Nanoparticle-Augmented Sonodynamic Therapy (SDT): breaking the depth shallow of photoactivation. Adv. Mater. doi:10.1002/adma.201602012 (2016) (Epub ahead of print).

60 Serpe L FF, Canaparo R. Nanosonotechnology: the next challenge in cancer sonodynamic therapy. Nanotechnol. Rev. 1(2), 173–182 (2012).

• A review on the different aspects related to nanotechnology that might well be able to improve the anticancer sonodynamic approach.

61 Costley D, Mc Ewan C, Fowley C et al. Treating cancer with sonodynamic therapy: a review. Int. J. Hyperthermia 31(2), 107–117 (2015).

62 Serpe L GM, Canaparo R, Dosio F. Targeted treatment of folate receptor-positive platinum-resistant ovarian cancer and companion diagnostics, with specific focus on vintafolide and etarfolatide. Pharmacogenomics Pers. Med. 7, 31–42 (2014).

63 Trachootham D, Alexandre J, Huang P. Targeting cancer cells by ROS-mediated mechanisms: a radical therapeutic approach? Nat. Rev. Drug Discov. 8(7), 579–591 (2009).

64 Sazgarnia A, Shanei A, Eshghi H, Hassanzadeh-Khayyat M, Esmaily H, Shanei MM. Detection of sonoluminescence signals in a gel phantom in the presence of Protoporphyrin IX conjugated to gold nanoparticles. Ultrasonics 53(1), 29–35 (2013).

•• Represents one of the first studies aimed to support the hypothesis that sonoluminescence ultrasonically induced may account for the sonodynamic anticancer effects.

65 Wang X, Chen H, Zheng Y et al. Au-nanoparticle coated mesoporous silica nanocapsule-based multifunctional platform for ultrasound mediated imaging, cytoclasis and tumor ablation. Biomaterials 34(8), 2057–2068 (2013).

66 El-Hussein A, Mfouo-Tynga I, Abdel-Harith M, Abrahamse H. Comparative study between the photodynamic ability of gold and silver nanoparticles in mediating cell death in breast and lung cancer cell lines. J. Photochem. Photobiol. B 153 67–75 (2015).

67 Zhang H, Shan Y, Dong L. A comparison of TiO2 and ZnO nanoparticles as photosensitizers in photodynamic therapy for cancer. J. Biomed. Nanotechnol. 10(8), 1450–1457 (2014).

68 Chirico G, Pallavicini P, Collini M. Gold nanostars for superficial diseases: a promising tool for localized hyperthermia? Nanomedicine (Lond.) 9(1), 1–3 (2014).

69 Pedrosa P. RVR, Alexandra Fernandes A, Baptista PV. Gold nanotheranostics: proof-of-concept or clinical tool? Nanomaterials 5(26), 1853–1879 (2015).

70 Yildirimer L, Thanh NT, Loizidou M, Seifalian AM. Toxicology and clinical potential of nanoparticles. Nano Today 6(6), 585–607 (2011).

71 Wen D. Nanoparticle-related heat transfer phenomenon and its application in biomedical fields. Heat Transfer Engineering 34(14), 1171–1179 (2013).

•• An important review supporting how the combination of GNP with ultrasound might be a promising strategy for future medical applications.